

Interplay between non equilibrium and equilibrium spin torque using synthetic ferrimagnets

Christian Klein

*SPSMS, UMR-E 9001 CEA / UJF-Grenoble 1, INAC, Grenoble, F-38054, France,
Physikalisches Institut, Universität Karlsruhe (TH), Wolfgang-Gaede Strasse 1, 76131 Karlsruhe, Germany*

Cyril Petitjean and Xavier Waintal

SPSMS, UMR-E 9001 CEA / UJF-Grenoble 1, INAC, Grenoble, F-38054, France

(Dated: April 11, 2012)

We discuss the current induced magnetization dynamics of spin valves $F_0|N|SyF$ where the free layer is a synthetic ferrimagnet SyF made of two ferromagnetic layers F_1 and F_2 coupled by RKKY exchange coupling. In the interesting situation where the magnetic moment of the outer layer F_2 dominates the magnetization of the ferrimagnet, we find that the sign of the effective spin torque exerted on the free middle layer F_1 is controlled by the strength of the RKKY coupling: for weak coupling one recovers the usual situation where spin torque tends to, say, anti-align the magnetization of F_1 with respect to the pinned layer F_0 . However for large coupling the situation is reversed and the spin torque tends to align F_1 with respect to F_0 . Careful numerical simulations in the intermediate coupling regime reveal that the competition between these two incompatible limits leads generically to spin torque oscillator (STO) behavior. The STO is found in the absence of magnetic field, with very significant amplitude of oscillations and frequencies up to 50 GHz or higher.

PACS numbers: 72.25.Ba, 75.47.-m, 75.70.Cn, 85.75.-d

Since the first successful experimental manipulation of magnetic configurations by spin-polarized currents [1, 2], the interest in spintronics devices entirely controlled by electrical currents has rapidly increased [3–10, 12, 13]. The key concept behind these experiments is the notion of spin transfer torque (STT) predicted by Slonczewski [14] and Berger [15]: a current gets spin polarized by a first (pinned) magnetic layer and then transfers some of its polarization to a second free layer, hence exerting a torque on its magnetization. As a result the magnetization can switch to a different static configuration [2, 3] or even to a dynamical stationary regime where the magnetization of the free layers shows a sustained precession [4–7]. This dynamical regime, known as the spin torque oscillation (STO), allows to convert a dc voltage into a microwaves signal at several GHz and has a real potential for applications (nanoscale microwave source or detector, high frequencies possibly above CMOS technology, narrow band). There are still technological issues with STO based devices, however, such as very limited output power and the need of rather strong external fields. Indeed, the main mechanism for producing STO is based on a detailed tuning of the angular dependence of the spin torque [5] and requires the use of an external magnetic field. Recently, different mechanisms have emerged to enable STO behavior in the absence of external field: the first approach [9] relies on the precession of a non uniform magnetic structure, a magnetic vortex, that can be excited at sub GHz frequencies; a second approach [8, 16] uses a strongly asymmetric spin valve to increase the anharmonicity of the angular dependence of the spin torque, leading to the so-called “wavy” behavior

of the STT [16–19]. Other approaches use an orthogonal polarizer [10] or a perpendicular free layer [11, 12].

In this letter we propose an entire new mechanism which naturally induces strong STO behavior, even in the absence of magnetic field, using a synthetic ferrimagnet (SyF) as the free layer of the spin valve. The SyF is made of two ferromagnetic layers coupled through anti-ferromagnetic RKKY exchange interaction [20–22]. Here, we predict that by simply tuning the effective strength of the RKKY exchange coupling (through the different thicknesses of the layers for instance), the *sign* of the effective STT can be changed. At intermediate effective coupling, the STT generically induces strong STO behavior irrespectively of the presence of applied magnetic field.

In the following we first provide a simple physical picture that captures the essential features of our setup. Our main prediction uses very general conservation arguments and should therefore be quite robust and independent of the details of the model. In a second step, we provide more quantitative arguments to describe the strong coupling regime. Last, we present a detailed numerical study of the phase diagram of our model. We find strong STO behavior at rather large frequencies in a wide portion of the phase diagram hinting that SyF based STOs could be good candidates for application purposes.

Physical mechanism. We consider a nanopillar spin valve $F_0|N_0|SyF$ made of a pinned ferromagnetic layer F_0 and a free synthetic ferrimagnetic layer $SyF = F_1|N_1|F_2$ (where N_0 and N_1 are normal spacers), see Fig. 1a for a cartoon of the full stack. Upon injecting a current density j through the nanopillar, a spin torque τ is exerted

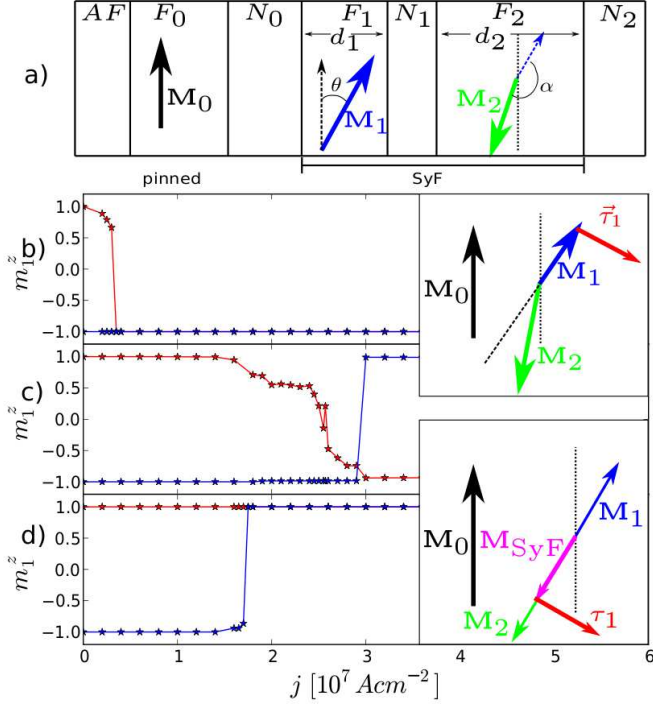


Figure 1: Panel (a) is a cartoon of the magnetic multilayer stack, in which \mathbf{M}_i is the magnetization of the layer F_i . The angle between \mathbf{M}_1 and \mathbf{M}_0 (\mathbf{M}_2) is respectively θ (α). Panels (b,c,d) show the stationary magnetization m_1^z along \mathbf{M}_0 as a function of the current density j in $\text{A}\cdot\text{cm}^{-2}$, for a stack with $d_1 = 2$ nm, $d_2 = 4 d_1$ and three different coupling strength J ; (b) weak coupling limit ($J = 0$), (c) Intermediate coupling limit ($J = -10^{-3} \text{ J}\cdot\text{m}^{-2}$) (d) Strong coupling limit ($J = -6 \cdot 10^{-3} \text{ J}\cdot\text{m}^{-2}$) Upper (Lower) inset : Sketch of the torque $\boldsymbol{\tau}_1$ action on \mathbf{M}_1 (\mathbf{M}_{SyF}) for the weak (strong) coupling regime.

on the magnetic moments of the layers [23]. This torque has been extensively discussed in the literature and can be strong enough to destabilize the initial magnetic configuration. On the other hand, the magnetization \mathbf{M}_1 and \mathbf{M}_2 of F_1 and F_2 are coupled by an oscillatory exchange (RKKY) interaction J which is nothing but the spin torque present in the pillar *at equilibrium* [24, 25]. The coupling J is reminiscent of Friedel oscillations and typically behaves as $J \sim (\cos 2k_F d_N)/d_N$ where k_F is the Fermi momentum and d_N the width of the spacer N_1 . J can be tuned from negative (antiferromagnetic coupling) to positive (ferromagnetic coupling), hence the name "oscillatory". Here we focus on negative values of J which stabilize an anti-aligned configuration of \mathbf{M}_1 and \mathbf{M}_2 . The goal of this letter is to discuss new phenomena that arise from the competition between the equilibrium and the non equilibrium torques.

In order to gain a qualitative understanding of the underlying physics, let us discuss two extreme limits. We start from a configuration where \mathbf{M}_1 is aligned with \mathbf{M}_0

while \mathbf{M}_2 is anti-aligned, and inject electrons from the right. Upon crossing the pinned layer F_0 , the electrons get a polarization anti-parallel to \mathbf{M}_0 . Denoting \mathbf{J}_i the spin current (per unit surface) flowing in the normal layer N_i , we have $\mathbf{J}_0 = \hbar p j \mathbf{m}_0 / (2e)$ with $\mathbf{m}_0 = \mathbf{M}_0 / |\mathbf{M}_0|$ and p the polarization of the current ($0 \leq p \leq 1$). Let us focus on the weak coupling limit where $J \rightarrow 0$. When there is a finite angle θ between \mathbf{M}_0 and \mathbf{M}_1 , the spin current on the left \mathbf{J}_0 and right \mathbf{J}_1 of F_1 become different and a torque $\boldsymbol{\tau}_1 = \mathbf{J}_0 - \mathbf{J}_1$ is exerted on the magnetization of F_1 : conservation of angular momentum implies that whatever spin lost by the conducting electrons is gained by magnetic degrees of freedom [14]. This conservation of angular momentum reads,

$$\frac{\partial}{\partial t} \left[\frac{d_1 \mathbf{M}_1}{\gamma_1} \right] = \boldsymbol{\tau}_1 + \dots \quad (1)$$

where d_1 is the width of F_1 , γ_1 its gyromagnetic ratio and the \dots indicate other contribution to the dynamics (magnetic anisotropy, damping) to be discussed later (upper inset of Fig. 1). Ignoring (momentarily [26]) the role of F_2 , we arrive at $\partial \theta / \partial t = \gamma_1 \hbar p j \sin \theta / (2ed_1 |\mathbf{M}_1|)$ and recover the usual phenomenology of spin torque: the torque tends to stabilize the configuration where \mathbf{M}_1 is anti-parallel to \mathbf{M}_0 (or destabilize it if one reverses the sign of the current).

Let us now discuss how this picture is modified when one considers the opposite strong coupling $J \rightarrow -\infty$ limit. Upon switching on J , the exchange energy (per unit surface of the pillar) $E_J = -J(\mathbf{m}_1 \cdot \mathbf{m}_2)$ induces a field like term in the RHS of Eq.(1) of the form $+\mathbf{J}\mathbf{m}_2 \times \mathbf{m}_1$. One needs also to consider the corresponding equation for the dynamics of \mathbf{M}_2 (see below Eq.(3) for the full model) and one obtains a potentially rich coupled dynamics for \mathbf{M}_1 and \mathbf{M}_2 . The situation simplifies in the limit where the exchange energy $J \rightarrow -\infty$ dominates: the relative configuration of \mathbf{M}_1 and \mathbf{M}_2 becomes frozen in the anti-aligned position. Conservation of angular momentum now leads to a spin torque on the total magnetic moment:

$$\frac{\partial}{\partial t} \left[\frac{d_1 \mathbf{M}_1}{\gamma_1} + \frac{d_2 \mathbf{M}_2}{\gamma_2} \right] = \boldsymbol{\tau}_1 + \dots \quad (2)$$

where we have used the fact that $\boldsymbol{\tau}_2 = \mathbf{J}_1 - \mathbf{J}_2$ vanishes when \mathbf{M}_1 and \mathbf{M}_2 are collinear. Note that the exchange field, which conserves the total angular momentum, redistributes the torque $\boldsymbol{\tau}_1$ on \mathbf{M}_1 and \mathbf{M}_2 so that they remain anti-aligned.

Eq.(2) allows two very different regimes: if $d_1 |\mathbf{M}_1| / \gamma_1 > d_2 |\mathbf{M}_2| / \gamma_2$ then the effective magnetization direction \mathbf{M}_{SyF} of the SyF layer points along \mathbf{M}_1 and the torque is very similar to the weak coupling regime. This case has attracted some attention recently both experimentally by Smith et al. [27] and theoretically by Balaz et al. [28]. Here, we focus on the other

limit $d_1|\mathbf{M}_1|/\gamma_1 < d_2|\mathbf{M}_2|/\gamma_2$ where \mathbf{M}_{SyF} points in the *opposite* direction as \mathbf{M}_1 (lower inset of Fig. 1). In this limit, the torque tends to stabilize the configuration where \mathbf{M}_{SyF} is anti-aligned with \mathbf{M}_0 hence where \mathbf{M}_0 and \mathbf{M}_1 are aligned: this is the opposite situation from the weak coupling $J \rightarrow 0$ limit.

To summarize, when going from $J \rightarrow 0$ to $J \rightarrow -\infty$, without changing the sign of the current, the torque tends to favor two different stationary situations. In the rest of this letter, we study this crossover in more details. In particular, we find that the intermediate coupling regime reveals interesting, STO like, dynamical behavior.

Model. We now turn to the modelisation of our system. The full stack we are considering has the form (see Fig. 1a): AF|F₀|N₀|F₁|N₁|F₂|N₂, where AF is an antiferromagnetic layer (typically IrMn) that pins the magnetization of F₀. We set our reference spin axis \mathbf{e}_z parallel to \mathbf{M}_0 . Magnetization dynamics is described by two coupled Landau Lifshitz Gilbert (LLG) equations that read (in SI units),

$$\frac{\partial \mathbf{m}_1}{\partial t} = \gamma_1 \mathbf{B}_1 \times \mathbf{m}_1 + \alpha_1 \mathbf{m}_1 \times \frac{\partial \mathbf{m}_1}{\partial t} + \frac{\gamma_1}{|\mathbf{M}_1|d_1} \boldsymbol{\tau}_1 \quad (3a)$$

$$\frac{\partial \mathbf{m}_2}{\partial t} = \gamma_2 \mathbf{B}_2 \times \mathbf{m}_2 + \alpha_2 \mathbf{m}_2 \times \frac{\partial \mathbf{m}_2}{\partial t} + \frac{\gamma_2}{|\mathbf{M}_2|d_2} \boldsymbol{\tau}_2, \quad (3b)$$

where $\mathbf{m}_i = \mathbf{M}_i/|\mathbf{M}_i|$ is the unit vector describing the magnetization orientation of the layer \mathbf{F}_i and α_i is the damping factor of the corresponding magnetic material. The effective field \mathbf{B}_i seen by the magnetization in the layer ($i = (1, 2)$) is

$$\mathbf{B}_i = \frac{K_u^i}{|\mathbf{M}_i|} [\mathbf{m}_i \cdot \mathbf{e}_z] \mathbf{e}_z + \frac{J}{|\mathbf{M}_i|d_i} \mathbf{m}_{\bar{i}}, \quad (4)$$

where $\bar{i} = 3 - i$ corresponds to the index of the other layer. The effective field includes an uniaxial anisotropy K_u^i field and the RKKY exchange field. In the physical regimes studied below, RKKY coupling is the dominating energy so that our results are rather insensitive to the presence of less important terms (for instance dipolar coupling between layers that we do not take into account). The spin torque $\boldsymbol{\tau}_i$ is calculated in the framework of CRMT (Continuous Random Matrix Theory) [16, 29]. CRMT is a semiclassical approach that generalizes Valet-Fert theory to non collinear situations. For discrete systems, It is formally equivalent to the generalized circuit theory [30] and is well adapted to the treatment of metallic magnetic multilayers.

Strong coupling limit. When the RKKY coupling is large, one can derive an effective LLG equation for the dynamics of the SyF. It reads,

$$\frac{\partial \mathbf{m}_1}{\partial t} = \gamma_{\text{eff}} \mathbf{B}_{\text{eff}} \times \mathbf{m}_1 + \alpha_{\text{eff}} \mathbf{m}_1 \times \frac{\partial \mathbf{m}_1}{\partial t} + \frac{\gamma_{\text{eff}}}{|\mathbf{M}_1|d_1} \boldsymbol{\tau}_1, \quad (5)$$

where the various effective parameters get renormalized as follows: $\gamma_{\text{eff}} = \gamma_1/(1 - \delta)$, $\alpha_{\text{eff}} = (\alpha_1 + \delta\alpha_2)/(1 - \delta)$,

$K_u^{\text{eff}} = K_u^1 + K_u^2 d_2/d_1$, $\mathbf{B}_{\text{eff}} = (K_u^{\text{eff}}/|\mathbf{M}_1|)[\mathbf{m}_1 \cdot \mathbf{e}_z] \mathbf{e}_z$ and the renormalization parameter δ has been defined as,

$$\delta = \frac{\gamma_1 |\mathbf{M}_2| d_2}{\gamma_2 |\mathbf{M}_1| d_1} \quad (6)$$

(Eq.(5) is obtained by calculating $\partial/\partial t[\mathbf{m}_1 + \delta \mathbf{m}_2]$ which cancels the RKKY contribution, and then setting $\mathbf{m}_2 = -\mathbf{m}_1$ and $\boldsymbol{\tau}_2 = \mathbf{0}$). From this equation we can clearly see the inversion of the sign of the effective torque $\gamma_{\text{eff}} \boldsymbol{\tau}_1$ discussed previously when $\delta > 1$.

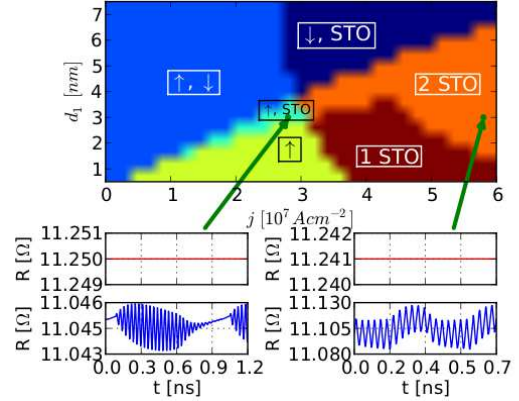


Figure 2: Upper: phase diagram of the system as a function of the current density j and the thickness d_1 for a fixed $\delta = 4$ and $J = -5 \cdot 10^{-3} \text{ J.m}^{-2}$. The various symbols indicate the observed stationary states in the corresponding region (defined by different colors): \uparrow (\downarrow) stands for $m_1^z = 1$ ($m_1^z = -1$), while *STO* corresponds to the presence a precessional state. In the *2 STO* region, two different *STO* states can be observed depending on the hysteresis history. Lower: Resistance R as function of time t for a pillar surface of 1000 nm^2 and $d_1 = 3 \text{ nm}$. Upper (lower) plots correspond to initial conditions in the up (down) configuration. Left panels: $j = 2.8 \cdot 10^7 \text{ A.cm}^{-2}$. Right panels: $j = 5.8 \cdot 10^7 \text{ A.cm}^{-2}$. The amplitude of the oscillation with the up initial condition is small and invisible on the scale of the graphics

Numerical simulations. Let us now go back to the full model Eq.(3) and study it numerically. We focus on a stack defined as IrMn₅|Py₅|Cu₁₀|Co_{d1}|Ru_{0.3}|Co_{d2}|Cu₁₀ where the index indicate the widths of the layers in nm. We have used $K_u^{\text{Co}} = 8 \cdot 10^4 \text{ J.m}^{-3}$, $M_{\text{Co}} = 1.42 \cdot 10^6 \text{ A.m}^{-1}$ and the transport parameters (spin resolved bulk resistivities, interface resistivities, spin flip lengths) have been taken from the database established in MSU and CNRS/Thales laboratory [31]. The coupling constant J can be tuned by changing the Ru thickness with typical values $J^{\text{Ru}} \approx -5 \cdot 10^{-3} \text{ J.m}^{-2}$ [21]. The torque and resistances have been calculated using CRMT and the corresponding parametrization (as a function of the angles θ and α , see Fig.1a) incorporated into our numerical LLG integrator.

A first set of curve is presented in Fig. 1 b,c and d where the stationary magnetization m_1^z along the z axis

is plotted against the current density j for three values of the coupling constant: small (b), intermediate (c) and large coupling (d). For small coupling (b), we recover the usual behavior of current induced magnetic reversal in spin valves: at zero current the system has two stable configurations where \mathbf{m}_1 is aligned ($m_1^z = 1$) or anti aligned ($m_1^z = -1$) with \mathbf{m}_0 . Upon injecting a strong positive current, one "pushes" toward the anti-aligned configuration which becomes stable above a critical value of the current density j ($0.5 \cdot 10^7 \text{ A.cm}^{-2}$ in this example). At large coupling (d), this hysteretic curve is reversed, in agreement with the arguments developed above. A very interesting regime is found at intermediate couplings (c) where one observes a rather large window where the stationary value of m_1^z corresponds to a finite angle between \mathbf{m}_0 and \mathbf{m}_1 , i.e. to a dynamical state where a sustained precession of \mathbf{m}_1 is present (with frequencies around 15 GHz in this example).

The coupling J can be varied by tuning the width d_N of the normal (Ru) spacer. However, this is not very easy to control in practice, as the oscillatory character of the RKKY interaction make this variation non monotonic. Alternatively, one can explore the phase diagram of our stack by varying the thickness d_1 for a fixed ratio $\delta = d_2/d_1$, hence varying the relative importance of bulk versus surface terms in the LLG equation. Fig. 2, shows the resulting phase diagram in the (j, d_1) plane for $\delta = 4$. The different symbols indicate the possible stationary states in the various regions of the phase diagram (defined by the various colors). The presence of two different symbols (most regions) indicate that depending on the hysteresis history, one or the other state is observed. In particular, in the 2 STO region, two different STO states can be observed depending, for instance, on the initial condition $m_1^z(t=0) = \pm 1$. These two different STO states merge upon entering the 1 STO region. We have investigated other stacks with different material parameters (not shown) and found very similar phase diagrams, including the presence of high frequency STO phases, as long as one remains in the $\delta > 1$ regime. We observe two kind of STO behaviors, as evident from the Resistance versus time $R(t)$ traces plotted in Fig. 2. When the amplitude of the oscillating signal is small (lower left of Fig. 2), we observe some beating behaviors with one well defined frequency and a second much smaller frequency less well defined (corresponding to the precession of the two layers respectively). When these two frequencies become closer, the time dependent signal gets bigger and $R(t)$ becomes much more sinusoidal indicating phase locking between the precessional dynamics of the two magnetizations \mathbf{m}_1 and \mathbf{m}_2 .

In the last Fig.3, we focus on the region of the phase diagram (lower right corner of Fig.2) where the amplitude of the STO signal is the highest. The upper curves show the amplitude of the time dependent signal while the lower curves show the corresponding frequency. We

find that this large angle STO phase, which is stable in the absence of magnetic field, leads to very high frequencies up to several tens of GHz while sustaining high precession angles (of the order of $\pi/6$). The observed high frequencies is tightly linked with the high value of the RRKY coupling which can be up to two orders of magnitude larger than typical anisotropy or Zeeman energies. Even if the relative angle between the two magnetizations of the synthetic ferrimagnet remain close to π , this gives rise to frequencies of several tens of GHz.

To conclude, we have shown that the interplay between equilibrium and non equilibrium torque in synthetic ferrimagnets based spin valves can lead to interesting physics and potentially a new route to high frequency STOs.

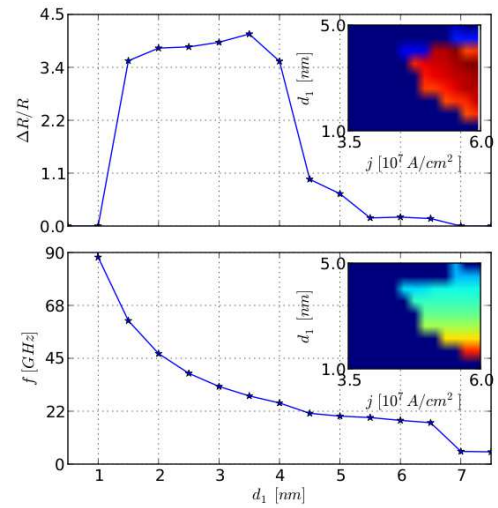


Figure 3: Upper plot: amplitude (in %) of the time dependent signal of the resistance as a function of d_1 for fixed $j = 6.10^7 \text{ A.cm}^{-2}$. Lower plot: idem for the main oscillating frequency of the resistance. Insets: corresponding colorplots in the (j, d_1) plane. $\delta = 4$ and $J = -5.10^{-3} \text{ J.m}^{-2}$.

We thank T. Rasing, W. Wulfhekel for very useful discussions. This work was supported by , CEA NanoSim program, CEA Eurotalent and EC Contract Macalo.

-
- [1] M. Tsoi, A. G. M. Jansen, J. Bass, W.-C. Chiang, M. Seck, V. Tsoi, and P. Wyder, Phys. Rev. Lett. **80**, 4281 (1998).
 - [2] E. Myers, D. Ralph, J. Katine, R. Louie, and R. Buhrman, Science **285**, 867 (1999).
 - [3] J. Katine, F. Albert, R. Buhrman, E. Myers, and D. Ralph, Phys. Rev. Lett. **84**, 3149 (2000).
 - [4] M. Tsoi, A. G. M. Jansen, J. Bass, W.-C. Chiang, V. Tsoi, and P. Wyder, Nature **406**, 46 (2000).
 - [5] S. I. Kiselev, J. C. Sankey, I. N. Krivorotov, N. C. Emley, R. J. Schoelkopf, R. A. Buhrman, and D. C. Ralph, Nature **425**, 380 (2003).

- [6] W. Rippard, M. Pufall, S. Kaka, S. Russek, and T. Silva, Phys. Rev. Lett **92**, 027201 (2004).
- [7] I. N. Krivorotov, N. C. Emley, J. C. Sankey, S. I. Kiselev, D. C. Ralph, and R. A. Buhrman, Science **307**, 228 (2005).
- [8] O. Boulle, V. Cros, J. Grollier, L. G. Pereira, C. Deranlot, F. Petroff, G. Faini, J. Barna, and A. Fert, Nature Phys. **3**, 492 (2007).
- [9] V. S. Pribiag, I. N. Krivorotov, G. D. Fuchs, P. M. Braganca, O. Ozatay, J. C. Sankey, D. C. Ralph, and R. A. Buhrman, Nature Phys. **3**, 498 (2007).
- [10] D. Houssameddine, U. Ebels, B. DelaëT, B. Rodmacq, I. Firastrau, F. Ponthenier, M. Brunet, C. Thirion, J. P. Michel, L. Prejbeanu-Buda, et al., Nature Mat. **6**, 447 (2007).
- [11] G. Consolo, L. Lopez-Diaz, L. Torrez, G. Finocchio, A. Romeo, and B. Azzerboni, Appl. Phys. Lett. **91**, 162506 (2007).
- [12] W. H. Rippard, A. M. Deac, M. R. Pufall, J. M. Shaw, M. W. Keller, S. E. Russek, and C. Serpico, Phys. Rev. B **81**, 014426 (2010).
- [13] M. Madami, S. Bonetti, G. Consolo, S. Tacchi, G. Carlotti, G. Gubbiotti, F. B. Mancoff, M. A. Yar, and J. Åkerman, Nature Nanotechnology **6**, 635 (2011). Nature Nanotechnology **6**, 635638 (2011)
- [14] J. C. Slonczewski, JMMM **62**, L1 (1996).
- [15] L. Berger, Phys. Rev. B **54**, 9353 (1996).
- [16] V. S. Rychkov, S. Borlenghi, H. Jaffres, A. Fert, and X. Waintal, Phys. Rev. Lett. **103**, 066602 (2009).
- [17] J. Manschot, A. Brataas, and G. Bauer, Phys. Rev. B **69**, 092407 (2004).
- [18] J. Barnaś, A. Fert, M. Gmitra, I. Weymann, and V. Dugaev, Phys. Rev. B **72**, 024426 (2005).
- [19] M. Gmitra and J. Barnas, Phys. Rev. Lett. **96**, 207205 (2006).
- [20] S. S. P. Parkin, N. More, and K. P. Roche, Phys. Rev. Lett. **64**, 2304 (1990).
- [21] S. Parkin, Phys. Rev. Lett. **67**, 3598 (1991).
- [22] P. Bruno and C. Chappert, Phys. Rev. B **46**, 261 (1992).
- [23] $j > 0$ corresponds to injecting an electrons from the right.
- [24] J. Slonczewski, Phys. Rev. B **39**, 6995 (1989).
- [25] X. Waintal and P. W. Brouwer, Phys. Rev. B **65** 054407(2002).
- [26] In the case considered here, the effect of τ_2 will only slightly increase the predicted effect.
- [27] N. Smith, S. Maat, M. J. Carey, and J. R. Childress, Phys. Rev. Lett. **101**, 247205 (2008).
- [28] P. Baláz and J. Barnaś, Phys. Rev. B **83**, 104422 (2011).
- [29] S. Borlenghi, V. S. Rychkov, C. Petitjean, and X. Waintal, Phys. Rev. B **84**, 035412 (2011).
- [30] G. E. W. Bauer, Y. Tserkovnyak, D. Huertas-Hernando, and A. Brataas, Phys. Rev. B **67**, 094421 (2003).
- [31] H. Jaffres private communication.